PAPER Nr.: 64

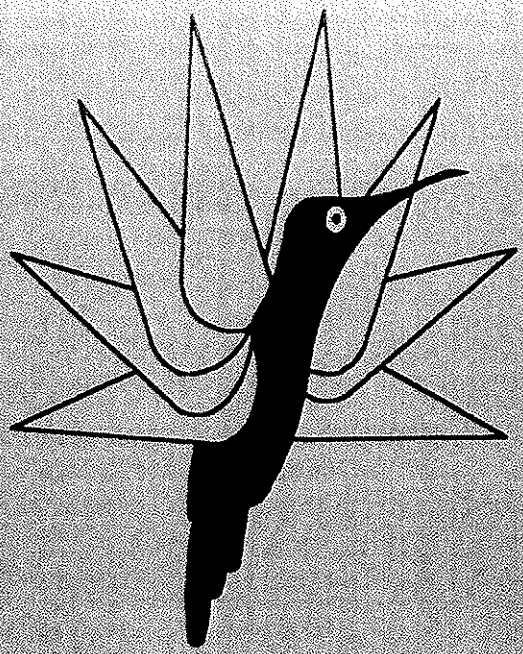

ACTIVE CONTROL OF GROUND AND AIR RESONANCE INCLUDING TRANSITION FROM GROUND TO AIR

BY

CH. KESSLER AND G. REICHERT

INSTITUTE OF FLIGHT MECHANICS
TECHNICAL UNIVERSITY OF BRAUNSCHWEIG
GERMANY

TWENTIETH EUROPEAN ROTORCRAFT FORUM
OCTOBER 4 - 7, 1994 AMSTERDAM

Printed by the Technical Highschool Haarlem

ACTIVE CONTROL OF GROUND AND AIR RESONANCE INCLUDING TRANSITION FROM GROUND TO AIR

Ch. Kessler, G. Reichert

Institute of Flight Mechanics
Technical University of Braunschweig, Germany

Abstract

Articulated and soft–inplane hingeless rotor helicopters are susceptible to certain self–excited instabilities called ground and air resonance. These instabilities derive from the coupling of rotor and body degrees of freedom and are well known for a long time. In general there is a good basic understanding how to avoid these instabilities. But since it became more and more desirable to focus rotor design on aerodynamic features and flight performance these aeromechanical instabilities gain new importance due to the difficulties to provide the required damping. On the other hand active control offers the possibility for an artificial stabilization of ground and air resonance. Meanwhile many modern helicopters are fitted with stabilization systems to improve handling qualities and it has been discussed already to use these active means to overcome mechanical instabilities.

A fully spatial model is used including dynamic inflow as well as flap–lag–coupling. The coupled set of nonlinear differential equations is included in a numerical simulation computer code and after an analytical linearization in a stability computation routine.

The main emphasis of this paper is to demonstrate the potential of active control. The matrices of the state space representation are used for optimizing feedback gains. However, this method is problematic for transient from ground to air due to the rapid change of system characteristics. Numerical simulation results will demonstrate the transient behavior.

Notations and Abbreviations

a	m	blade hinge offset or lever
d	kg/s	damping constant of simplified model
d_ζ	Nms	lead–lag damping constant
D	–	damping ratio
F	N	rotor thrust, force
G_{xi}		feedback gain for state variable x_i
h	m	offset of rotor hub from c.g.
I	kgm^2	moment of inertia
k	N/m	spring constant of simplified model
k_β, k_ζ	Nm	flap–, lag–spring constants
m	kg	body mass
p, q, r	rad/s	body rates
Q	N	shear force for simplified model
u, v, w	m/s	body velocities
w_i	m/s	induced velocity
x, y, z	m	coordinates
β	$^\circ$	flap angle
ε	m	small parameter
ζ	$^\circ$	lead–lag angle
ϑ	$^\circ$	blade pitch angle
φ	$^\circ$	feedback phase
σ	$^\circ$	real part of eigen value
Φ, Θ, Ψ	$^\circ$	EULER angles
ψ	$^\circ$	blade azimut angle
Ω	rad/s	rotor rotational speed, forcing frequency
ω, ω_0	rad/s	eigen frequency

0, d	collective, differential
C, S	cyclic sine and cosine
crit, nom	critical, nominal
l, r	left, right
lin, nl	linear, nonlinear
prog, reg	progressing, regressing
$\hat{(\,)}$	amplitude
$\dot{(\,)}$	$= \partial(\,)/\partial t$

1 Introduction

Since the introduction of hingeless rotor helicopter by MBB in the sixties much R&D effort has focused on these rotor types. As a consequent development of hingeless rotors bearingless rotors will enter helicopter service (EC 135, MDX Explorer). The main advantages of such rotor systems compared to articulated rotors are mechanical simplification, reduced drag, weight, parts and maintenance costs, higher moment capability, determined by the flapping stiffness,

and faster moment setup due to cyclic control inputs and therefore better handling qualities [6]. There are two *successfully flown hingeless rotor concepts*. The Boelkow-System makes use of elastic coupling effects, the other (WG 13) prevents these couplings. Important parameters in designing hingeless/bearingless rotors are blade flapping and lagging frequencies. Both rotor systems can be divided into two distinct groups depending on the inplane frequency: soft–inplane rotors with $\omega_\zeta/\Omega < 1$ and stiff–inplane rotors $\omega_\zeta/\Omega > 1$. Low inplane rotor loads can only be achieved by using soft–inplane rotors. As a consequence of this modern hingeless/bearingless rotors are designed as soft–inplane, but are susceptible to ground and air resonance. To prevent these instabilities sufficient lead–lag damping has to be provided. This can be done either by adding dampers or by using structural damping and damping from aeroelastic couplings or by Active Control Technology (ACT). The introduction of Fly–by–Wire technology and digital control systems of future helicopter generations offers a broad range of different ACT concepts.

The enormous control power inherent in hingeless/bearingless rotor concepts makes feedback control an effective means of augmenting system stability. With this in mind several authors examined the possibilities of suppressing ground and air resonance by ACT using a conventional swashplate. Early work was done by YOUNG et al. [12]. The instable ground resonance mode was found out to be a roll mode. Feedback of roll attitude and roll rate was effective in suppressing a growing instability. The same turned out for air resonance in hover. A more detailed study was made by STRAUB and WARMBRODT [5]. The analytical model used was a hingeless rotor system with body pitch and roll as well as body longitudinal and lateral translation. The rotor blades were assumed to be rigid rotating against spring and damper restraints about a common flap–lag–hinge. Flap–lag–coupling was included but no dynamic inflow. Dynamic inflow is mentioned to be an important modelling aspect for stability and control investigations [3]. The regressing lag mode was denoted to become instable. Several feedback loops were investigated including cyclic flap and lead–lag, body pitch and roll states. Two mechanisms were mentioned to stabilize ground resonance: first, controlling body pitch and roll through flapping moments, secondly, augmenting lead–lag damping through Coriolis coupling with blade flapping. Since the model showed only one mild instability ($\sigma = 0.145/s$) stability could be achieved throughout the considered range of rotor rotational speed with appropriate chosen gains and phases. Scheduling feedback phase was found out to *maximize damping augmentation*.
In a second paper STRAUB [16] used the same mathematical model to study linear optimal control. This time he examined a four bladed articulated rotor helicopter. The optimal gains were obtained from the solution of RICATTI equation. Several suboptimal controllers were tested. They were achieved by removing the feedback loops of the optimal controller step by step. Chosing appropriate feedback signals resulted in sufficient lead–lag damping of the closed loop system throughout the considered rotor speed range.
Finally REICHERT and ARNOLD [8] picked up the idea of controlling ground resonance through a conventional swashplate and compared these results with an Individual Blade Control (IBC) approach. They used a spatial helicopter model including all six body DOF. The four bladed hingeless rotor was modelled similar to [5]. Dynamic inflow was again neglected. The IBC principle (lag damping augmentation through feedback of lead–lag states in the rotating frame and controlling lead–lag through Coriolis forces) resulted in poor aeromechanical stability for the instable pitch mode compared to body pitch feedback results.
TAKAHASHI and FRIEDMANN [10] studied active control of air resonance applying linear quadratic optimal control theory. A comparison of full state feedback was made to partial state feedback. Feedback of only body states resulted in poor lead–lag damping and in a destabilization of the progressing lead–lag mode.

None of these authors considered the transient behavior from ground to air at high thrust levels. YOUNG et al. [12] marked this area in their figures with a "visual remainder" at $F/mg = 90\,\%$. ORMISTON determined ground and air resonance characteristics of a hingeless rotor helicopter. He compared the modes that participate in air resonance phenomenon to the more familar modes of ground resonance. He reduced body frequencies due to lowering landing gear stiffness and examined thus take–off condition, still using a linear model. Capturing transition affords the modelling of a nonlinear landing gear. The landing gear represented by a spring/damper system cannot transmit tension from the fuselage to the ground. Due to this the landing gear may lose partially ground contact during transition.

The aim of this paper is first to include such a nonlinear landing gear model and to compare the helicopter behavior to a model with a linear landing gear. Secondly, the use of ACT to prevent ground resonance

and its consquences to the helicopter in hover should be further studied.

2 Mathematical Model

The mathematical model used in this study is similar to those of ref. [8]. The spatial helicopter model is shown in fig. 1 and includes all six body DOF. The rotor hub is located directly above the fuselage c.g. The blades are assumed to be rigid undergoing flapping and lagging motion rotating against linear spring and damper restraints. Lead–lag and flap motion have the same virtual hinge in common with a distinct offset a from the rotor center. Structural flap–lag coupling, precone and linear twist can be included. Aerodynamic rotor blade forces and moments are based on a linear two–dimensional blade element theory. Fuselage aerodynamics are included in the form of a linear derivative approach. Tail rotor dynamics are not included.
In addition to ref. [8] low frequency unsteady aerodynamics (dynamic inflow) are included. This is mentioned to be an important modelling aspect in literature [3, 7, 9, 10]. However, blade torsion is neglected. The landing gear is modelled in two different manners. The *linear* approach is realized by a system of linear springs and viscoelastic dampers at each of the four landing gear levers pointing in all three directions and with distinct offsets from the fuselage c.g. The *nonlinear* approach is modelled by a system of springs and dampers at each of the four landing gear levers, too, but no tension can be transmitted from the fuselage to the ground. The modelling will be described in detail later on. With this, transient behavior can be studied. For clearness: a conventional linearization and eigen value analysis cannot be performed. An analysis can only be performed by integrating the differential equations numerically.

All differential equations were derived by using the symbolic manipulation programs DERIVE and REDUCE, considering all geometric nonlinearities. These equations were included in a time integration routine to compute the time history results used later on. To simplify designations the two models with the two different landing gear descriptions are refered as the *linear model* and the *nonlinear model* respectively depending upon the landing gear modelling. A linearization was made for the helicoper model with the linear landing gear system, using the same tools. No ordering scheme was used, so all terms are retained in the analysis. A multiblade transformation was performed. For a four bladed helicopter this is done by

$$\beta_k = \beta_0 + \beta_C \cos\psi_k + \beta_S \sin\psi_k + \beta_d \,, \quad (1)$$

$$\zeta_k = \zeta_0 + \zeta_C \cos\psi_k + \zeta_S \sin\psi_k + \zeta_d \,. \quad (2)$$

Assuming all blades identical and restricting the analysis to hover condition this results in 14 second order (body/rotor) and three first order (inflow) differential equations with constant coefficients. After a state space transformation one gets 31 first order differential equations with constant coefficients in matrix form:

$$\dot{\underline{x}} = \underline{\underline{A}}\,\underline{x} + \underline{\underline{B}}\,\underline{u} \,, \quad (3)$$

with the states $\underline{x} = [\dot{\beta}_0, \dot{\beta}_C, \dot{\beta}_S, \dot{\beta}_d, \beta_0, \beta_C, \beta_S, \beta_d, \dot{\zeta}_0, \dot{\zeta}_C, \dot{\zeta}_S, \dot{\zeta}_d, \zeta_0, \zeta_C, \zeta_S, \zeta_d, u_{ks}, v_{ks}, w_{ks}, x, y, z, p_s, q_s, r_s, \Phi, \Theta, \Psi, w_{i0}, w_{iC}, w_{iS}]^T$ and three control inputs $\underline{u} = [\vartheta_0, \vartheta_C, \vartheta_S]^T$.
The data used in this study correspond to a four bladed soft inplane helicopter somewhat similar to the ECD Bo 105 with a high landing gear. REICHERT and ARNOLD [8] have done their studies for the same helicopter, but with a conventional landing gear, resulting in a higher stiffness and therefore in higher body frequencies. They mentioned the coupled translatory/rotatory modes to be $\omega_{x/\Theta} = 20.7 rad/s$ and $\omega_{x/\Phi} = 23.9 rad/s$, resulting in coupling with lead–lag motion at rotor speeds far beyond the nominal speed. For the Bo 105 helicopter with the high landing gear it is known that a critical rotor speed occurs below the nominal value, see fig. 2. This seems to be a more interesting case, since the rotor has to pass this critical rotor speed, bringing rotor to nominal speed. The data of the nominal configuration are listed below.

Fuselage Data			Rotor Data		
m	= 1906	kg	Ω_{nom}	= 44.5	$1/s$
I_{xx}	= 1515	kgm^2	R	= 4.91	m
I_{yy}	= 4863	kgm^2	m_{bl}	= 23.4	kg
I_{zz}	= 3869	kgm^2	a	= 0.76	m
I_{xz}	= 640	kgm^2	ϑ_{tw}	= -1.6	$°/m$
$\omega_{x/\Theta}$	= 12.2	$1/s$	β_{pc}	= 2.5	°
$\omega_{x/\Phi}$	= 17.8	$1/s$	ω_β	= 1.12	$1/s$
$D_{x/\Theta}$	= 5.6	%	ω_ζ	= 0.67	$1/s$
$D_{x/\Phi}$	= 4.6	%	d_β	= 0	Nms
			d_ζ	= 60	Nms
			h	= 1.5	m

Table 1: Data of Nominal Configuration

The low body frequencies result in a coalescense of regressing lead–lag with the body x/Θ–mode at $\Omega = 91\%\,\Omega_{nom}$ and with y/Φ–mode at $\Omega = 112\%\,\Omega_{nom}$. The lead–lag damping was chosen from fig. 3. This figure shows the damping ratio D_ζ versus the lead–lag damping constant d_ζ of the isolated lead–lag mo-

tion in the rotating system and the regressing lead–lag mode in the body fixed system for zero thrust and medium thrust at $\Omega = 91\%\,\Omega_{nom}$. The chosen value $d_\zeta = 60\,Nms$ provides about 1% of critical damping for the isolated lead–lag motion which is not sufficient to avoid a ground resonance instability for the coupled system even at low thrust (low collective pitch).

Taking the data from tab. 1 an eigen value calculation for the helicopter on ground was performed varing the rotor speed from 0% to $140\%\Omega_{nom}$ at zero thrust. Real and imaginary parts of the eigen values are shown in fig. 4. The eigen modes were identified at nominal rotor speed. The 31 states result in 15 complex conjugated values and one real eigen value. The figure clearly shows the curve for the regressing lead–lag motion of a soft inplane hingeless rotor helicopter whereas the curve for the progressing lead–lag mode is not fully visible. The single body modes convert into progressing lead–lag and afterwards back into the next higher body frequency. The collective lead–lag mode couples with body yawing motion. Furthermore, the figure shows low frequency eigen modes for regressing flap and dynamic inflow as denoted by JOHNSON [2]. Both modes are highly coupled. Another coupling of rotor and body modes exists between body vertical translation with collective flap. The relatively low eigen frequencies of body x/Θ and y/Φ modes result in a coalescense of the regressing lead–lag eigen frequency at 91% and $112\%\Omega_{nom}$, respectively. A third frequency cross–over is detected at about $125\%\Omega_{nom}$, which will not be considered furtheron. At these three points the regressing lead–lag mode couples with the body modes. Due to the coupling new modes arrise, two for each point of frequency coalescense, whereas the one is stabilized and the other is destabilized. In all three cases an instability exists characterizing the ground resonance case. For clearness: it cannot be said wether the body modes or regressing lead–lag become unstable as can be read by several authors investigating ground and air resonance. The instability is due to a coupling of eigen modes and one of the new coupled eigen modes becomes unstable.
A further eigen analysis was performed for the helicopter in hover for a rotor speed range from 80% to $120\%\Omega_{nom}$. The results are shown in fig. 5. The considered rotor speed ranges of fig. 4 and 5 are only of an academic interest. Now, as the helicopter is airborne, the restoring landing gear forces drop and the body frequencies are determined by the rotor blade flapping stiffness resulting in low frequency rigid body modes. The modes are denoted by using conventional flight mechanical notations. As can be seen from fig. 5 the helicopter is free from air resonance, which is in correlation with results from EWALD [1]. A weak instability exists for the Phugoid motion typical for a helicopter in hover. Due to the high equivalent hinge offset the flapping stiffness increases with rotor speed. The body modes become faster and significant coupling occurs between the body rotational modes and the flapping modes producing new oscillatory modes, see [3]. Especially the body roll mode, which is faster than the body pitch mode due to the lower body inertia, combines itself with the flapping motion.

As the two extreme operating conditions (helicopter on ground, 0% airborne, and helicopter in hover) have been stated it has to be examined what happens inbetween these conditions. This is of high interest especially for high thrust conditions when the helicopter is still on ground. To get an idea whatever happens in this region a simplified model is considered in chapter four to investigate transient behavior. In the same chapter simulation results using the spatial model with the two mentioned landing skid types will demonstrate differences during transition from ground to air for some chosen operating conditions. Before this the potential of active control of ground resonance is to be considered and the consequences of the optimized controllers on the handling qualities for the helicopter in hover will be discussed.

3 Active control of ground resonance

In stability– and control–theory signal–flow diagrams are used to gain physical insight to the investigated system. These diagrams can be drawn from the state space representation. They keep the same information but can be better understood than differential equations. The effects of feedback loops on the dynamic behavior can be discussed in a very simple manner. It is known from conventional control theory that a feedback loop across one integrator increases system damping whereas a feedback loop across two integrators changes the eigen frequency.

Fig. 6 shows the signal flow diagram for the helicopter on ground or in a hover condition. To reduce complexity those states and paths are only retained, known to be sufficient to describe ground and air resonance behavior of a hingeless rotor helicopter [2, 15]. The diagram breaks up into three dynamic blocks representing rotor, body and inflow dynamics. Inputs are sine and cosine blade pitches. The diagram clearly shows that flap and lead–lag motion are highly coupled due to aerodynamic and inertial effects. Flapping and dy-

namic inflow influence each other whereas the coupling of lagging and dynamic inflow can be neglected. Weak paths exist from the cyclic inputs to body roll and pitch motion caused by small aerodynamic terms. These terms are included, since no ordering scheme has been used. Compared with the paths from the control inputs to cyclic flap and lag they are small.
For fixed wing airplanes the control inputs cause direct motions of the fuselage. In contrast to that for helicopters control inputs cause rotor rolling and pitching moments due to flapping and thus angular body motions. The relations are that ϑ_C mainly influences the lateral body motion and ϑ_S the longitudinal body motion.

Modern rotorcraft make use of feedback of body states to improve handling qualities, i.e. to stabilize the rotational DOF's and to add a comfortable amount of damping to the system. A simple controller structure is known as Stability Augmentation Systems (SAS) where pilot ond controller act on different paths in the system. The mechanism of SAS is to generate rotor roll and pitch moments by the use of cyclic inputs to achieve the desired rotational reactions. These devices are usually designed as limited authority and low frequency systems to avoid an interference with rotor dynamics. SAS offers a cost effective possibility to overcome mechanical instabilities such as ground and air resonance. Several authors investigated the effects of feedback of body states on ground and air resonance stability [5, 8, 9, 11, 16]. STRAUB and WARMBRODT [5] investigated the effects of single feedback loops in a sophisticated manner. REICHERT and ARNOLD picked up the idea of SAS and IBC investigating the potential of multivariable feedback loops. But still the consequences of the optimized controllers on handling qualities have to be discussed.
The feedback control structure can be found in fig. 7. A single body or multiblade rotor state is fed back to the cyclic control inputs after being amplified by the gain $-G_x$. The phase φ_x distributes the feedback signal between ϑ_C and ϑ_S. Multivariable feedback is achieved by adding further parallel loops.

A first simple approach was made to investigate the possibilities of active control of ground resonance. The rotor speed was set to $91\,\%\,\Omega_{nom}$ according to the ζ_{reg}–x/Θ instability. Thrust to weight ratio was layed down to 50 %. Pitch rate was fed back with a feedback phase $\varphi_q = 90°$ causing a pure ϑ_S input. Together with the sign convention from fig. 7 this leads to a negative feedback necessary for stabilizing the system. In ref. [5, 8] negative feedback was achieved by chosing appropriate feedback phases. The chosen phase for this study corresponds with a phase of 270° in [8]. As known from the root–locus–theory the eigen values move into the zeros of the transfer function q_S/ϑ_S for increasing gain. This is shown in fig. 8 where the region marked by the dashed box is plotted on the right hand side using a bigger scale. The eigen values were plotted as crosses × and the zeros as circles ○. As can be seen from fig. 8 the eigen values of the closed loop system move into the zeros. With this the slightly unstable $\zeta_{reg}/x/\Theta$ mode can be stabilized. Two aspects have to be mentioned restricting the success of this simple approach. The obtainable damping is limited, since a zero occurs right beside the imaginary axis in the left plane. But, in the same manner as the instable mode is stabilized ζ_{prog} is destabilized. This agrees with results from ref. [3]. Differences are due to the coupling of lead–lag and body x/Θ mode in this study. Since the instable $\zeta_{reg}/x/\Theta$ mode crosses the imaginary axis at a feedback gain of $G_q = 0.29\,s$ and ζ_{prog} becomes unstable at $G_q = 0.59\,s$ stability is limited due to the latter aspect. Slightly better results could be obtained by an optimization of the feedback phase, but since the chosen phase is close to the optimal phase of pitch rate feedback mentioned in ref. [8] this does not seem to be very promissing. Thus a multivariable controller was designed.

Eight states were chosen as feedback signals: $\dot{\zeta}_C, \zeta_C, \dot{\zeta}_S, \zeta_S, p_S, \Phi, q_S$, and Θ. Rotor cyclic lead–lag states were included, since $\dot{\zeta}_C$ and ζ_S were mentioned in ref. [5] to augment system damping levels of a ζ_{reg}/Φ ground resonance instability. In the same study flap modes were not found out to be effective in stabilizing the system. Consequently, the flap state variables are not considered as feedback signals. The chosen feedback variables include all necessary information about rotor and body motion to suppress an oncoming instability for both $\zeta_{reg}/x/\Theta$, and $\zeta_{reg}/y/\Phi$ coupling. Scheduling the eight feedback gains and phases with rotor speed and thrust to weight ratio leads to system stability throughout all operating conditions for the linearized helicopter model. Optimization of feedback gains was done with a computer program described in [17] applying optimal output vector theory [14]. A linear integral quadratic performance index is used which penalizes the entire state vector and control time history. Thus, every state may be penalized although only the output variables are fed back

$$J = \int_0^\infty (\underline{x}^T \underline{\underline{Q}} \underline{x} + \underline{u}^T \underline{\underline{R}} \underline{u})\, dt\,. \tag{4}$$

In the output feedback problem, the performance index is dependent on the initial conditions of the state vector and the weighting matrices $\underline{\underline{Q}}$, and $\underline{\underline{R}}$. In order to eliminate the dependence on the initial states the performance criterion is averaged for a linearly independent set of initial states. The control vector is defined as

$$\underline{u} = -\underline{\underline{G}}\underline{y} = -\underline{\underline{GC}}\underline{x} \tag{5}$$

where $\underline{\underline{G}}$ is the gain matrix and $\underline{\underline{C}}$ the output matrix. Hence, the closed loop plant matrix becomes

$$\underline{\underline{A}}_c = \underline{\underline{A}} - \underline{\underline{BGC}}. \tag{6}$$

An optimization was performed using two different weighting matrices $\underline{\underline{Q}}$ for the same operating conditions mentioned above. The results are shown in fig. 9. The weighting matrix was first set to the identity matrix. The closed loop eigen values were plotted as diamonds $\diamond$. The second weighting matrix used different weightings. High weightings were chosen for the feedback states, low weightings for the well damped flap variables. These eigen values were marked by boxes $\square$. As can be seen in fig. 9 most of the eigen values remain unchanged. Only the important modes are affected by the active control device. With the simple weighting matrix sufficient damping levels can be achieved to the unstable $\zeta_{reg}/x/\Theta$ mode. Almost optimum is achieved with the second weighting matrix. Without changing the eigen frequencies significantly, damping levels of the stable $\zeta_{reg}/x/\Theta$ and the unstable $\zeta_{reg}/x/\Theta$ modes are almost the same. The amount of damping that the one $\zeta_{reg}/x/\Theta$ mode takes from its counterpart due to the coupling and therefore destabilized the system is shifted back by applying active control. This controller will be denoted C2 furtheron. A second controller was optimized setting rotor speed to $112\,\%\,\Omega_{nom}$ called C3. The same tendencies as mentioned before can be seen applying this controller to the unstable helicopter. The gains and phases are included in tab. 2 at the end of this paper.

Up to now rotor speed was kept constant to show the root placement in the complex plane. Fig. 10 shows the aeromechanical stability of the least stable mode plotted versus rotor rotational speed. Due to the medium thrust to weight ratio rotor speed range was limited to a minimum of $60\,\%\,\Omega_{nom}$. The thick line denotes the open loop case. The discussed closed loop cases with controller C2 and C3 are plotted as dashed and dashed–dotted lines, respectively. These graphs clearly show that an immense stabilization is achieved for $91\,\%\,\Omega_{nom}$ (C2) and $112\,\%\,\Omega_{nom}$ (C3) but a destabilization for controller C2 at $112\,\%\,\Omega_{nom}$ and vice versa. This indicates that scheduling of gains and phases is effective in order to suppress ground resonance at both points of instability. To get a controller providing stability throughout the rotor speed range without scheduling the method described by STRAUB [16] was applied. But, for this study no stabilization at all rotor speeds was achieved. This is caused by considering two unstable points of rotor/body coupling. In contrast to that STRAUB considered an articulated rotor with only one unstable ζ_{reg}/y coupling. To check this the lead–lag damping constant of tab. 1 was doubled. Thus, the instability at $91\,\%\,\Omega_{nom}$ vanished whereas the instability at $112\,\%\,\Omega_{nom}$ still remained but less unstable. Using the eight feedback variables a controller was optimized at nominal rotor speed. This simple controller was able to suppress ground resonance at all rotor speeds. The chosen value for the lead–lag damping constant in ref. [16] is more than five times the value of this study. But, the introduction of active control devices to stabilize aeromechanical instabilities only makes sense, if at least two requirements are satisfied. First, adverse effects on handling qualities have to be avoided. Secondly, the controller must be able to handle less damped systems. This seems to be necessary to avoid further tailoring of rotor blades in order to provide the rotor with a minimum of damping.

To make sure that stabilizing the helicopter for all rotor speeds is possible a controller was designed by changing gains and phases by hand and checking the controller efficiency with the eigen values plotted versus the entire rotor speed range. It turned out that feedback loops for u_{kS} and v_{kS} had to be added. With this stability throughout the entire rotor speed range was achieved. The aeromechanical stability is plotted as a thin solid line in fig. 10. This demonstrates that a stabilization without scheduling is possible. This controller will be termed C1 furtheron.

To check the consequences of the designed controllers C1 and C2 for the helicopter in hover the eigen values were calculated with and without controllers at nominal rotor speed and $F/mg = 100\,\%$. The results are plotted in fig. 11. Due to the high feedback gains for body pitch and roll states an immense destabilization of the lateral mode arises applying controller C2. Moreover, a dramatic destabilization of lateral mode and Phugoid with controller C1 can be seen. There is no doubt that these adverse effects have to be avoided. Switching the controller from a "ground resonance mode" to an "air resonance mode" seems to be problematic, since it takes the helicopter a very short time to become airborne and because of the transient behavior which will be discussed in the next section.

A better solution seems to be to add filters to the controller. This has to be discussed in further investigations.

4 Modelling of transient behavior

4.1 Simplified model for transition considerations

In this section the behavior of a simplified model with the above mentioned nonlinear spring/damper system is to be compared to those of a linear model. This model is shown in fig. 12 and has the rotational DOF Θ and the DOF of vertical translation z. The model is excited by the harmonic force $Q = \hat{Q} \sin \Omega t$. Thus, a forced response problem will be considered rather than a self–excited one. But, already from this simple model some fundamental conclusions can be drawn. The differential equations of the linear model can be easily written:

$$m\,\ddot{z} + 2\,d\,\dot{z} + 2\,k\,z = mg - F\,, \qquad (7)$$

$$I_\Theta\,\ddot{\Theta} + 2\,d\,a^2\,\dot{\Theta} + 2\,k\,a^2\,\Theta, = Q\,h\,, \qquad (8)$$

where h is the vertical distance between the c.g. and Q and a is the lever of the combined spring–damper–system to the c.g., respectively. Considering F to be a constant force, the stationary solution for z is:

$$z = (mg - F)/(2k)\,. \qquad (9)$$

Now, consider a spring–damper–system at each lever, which is not attached on the ground. Hence, this spring–damper–system cannot transfer tension from the body to the ground. The description of the spring characteristic becomes nonlinear. The differential equations are:

$$\begin{aligned} m\,\ddot{z} &+ \frac{1}{2}\,d\left(\dot{z}_r(1+\tanh\frac{z_r}{\varepsilon_2}) + \dot{z}_l(1+\tanh\frac{z_l}{\varepsilon_2})\right) \\ &+ \frac{1}{2}\,k\left(z_r + \sqrt{z_r^2+\varepsilon_1} + z_l + \sqrt{z_l^2+\varepsilon_1}\right) \\ &= mg - F \qquad (10) \\ I_\Theta\,\ddot{\Theta} &+ \frac{a}{2}\,d\left(\dot{z}_l(1+\tanh\frac{z_l}{\varepsilon_2}) - \dot{z}_r(1+\tanh\frac{z_r}{\varepsilon_2})\right) \\ &+ \frac{a}{2}\,k\left(z_l + \sqrt{z_l^2+\varepsilon_1} - z_r - \sqrt{z_r^2+\varepsilon_1}\right) \\ &= Q\,h \qquad (11) \end{aligned}$$

with

$$\begin{aligned} z_r &= z - a\,\Theta \\ z_l &= z + a\,\Theta\,. \end{aligned}$$

Describing the damper in the written manner, relaxation of the spring–damper–system can be approximately neglected. The equations show, that both DOF are coupled for the nonlinear model, whereas they are uncoupled for the linear one.

Now consider the same model with Θ–DOF only, where z is kept at the value given by equation (9). Variing the forcing frequency and plotting the amplitude $(\Theta_{max} - \Theta_{min})/2$ of the stationary oscillation shows again fig. 12. The ratio F/mg was set to 85%, the forcing amplitude $\hat{Q}$ to $1100N$. The linear model shows the well known behavior with the maximum amplitude at the resonance frequency $\Omega = \omega_\Theta$. The nonlinear model shows a different behavior: the maximum amplitude is about 2.5 times the value of the linear model and occurs at a lower forcing frequency. This can be interpreted as a reduction in system damping and eigen frequency. Due to the nonlinearity, the left slope of the curve is much steeper than the right slope. This behavior is typical for a system with a degressive spring characteristic [4]. For low and high forcing frequencies the curves of the linear and nonlinear model are identical.

The response curve was computed using a numerical integration routine to get the time history of the differential equations. The stationary oscillation was analysed to get the amplitude $(\Theta_{max} - \Theta_{min})/2$. During the integration the forcing frequency was varied from its lower to its upper value and back again. This is necessary since nonlinear systems may show jump phenomena which are explained in detail in ref. [4]. These phenomena can be described as follows: increasing the forcing frequency during time integration the amplitude suddenly jumps from a lower to a higher value at a certain frequency. A further increase of the forcing frequency leads to a continuous curve. Decreasing the forcing frequency the response jumps from a higher to lower value. For a degressive system treated in this study the first jump happens at a higher forcing frequency than the second jump. Between these two frequencies a region exists where the system can respond at least with three amplidudes. The third one is an unstable oscillation and cannot be computed with a numerical integration routine. In the above described response diagram the nonlinearities are not strong enough to cause the jump phenomenon. This is explained in the same figure.

The last part of fig. 12 (below) shows the forcing frequency for the maximum value $(\Theta_{max} - \Theta_{min})/2$ for increasing thrust to weight ratio. Curves for two forcing amplitudes $\hat{Q}$ are included in this figure. The horizontal line denotes the resonance frequency for the linear system. It does not depend upon $\hat{Q}$ and F/mg. This is different for the nonlinear system. First two lines for each $\hat{Q}$ exist. This is due to the above mentioned jump phenomenon. For low and high thrust to

weight ratio both curves coalescense. Secondly, increasing F/mg the forcing frequency for maximum amplitude $(\Theta_{max} - \Theta_{min})/2$ reduces smoothly approaching a certain value for both forcing amplitudes $\hat{Q}$. This value is given by $a\sqrt{k/(I_\Theta)}$ at $F/mg = 100\%$, since only one spring–damper–system at each time has ground contact. Computing the response diagram for the nonlinear model at $F/mg = 100\%$ and for the linear model reducing spring stiffness k and damping constant d by $1/2$ leads to identical results. Thus, for low and high F/mg the nonlinear model seems to behave like a linear one.

Fig.13 compares the response diagram of the Θ–DOF model to that of the z–Θ–DOF model for $F/mg = 70\%$. The jump phenomenon can be seen for both models. At a forcing frequency of 10 $1/s$ the amplitude $(\Theta_{max} - \Theta_{min})/2$ jumps from the lower branch of the curve to the upper branch and at about 9.3 $1/s$ back to the lower branch again. The mentioned unstable solution is drawn as a dashed line and can be regarded as a fictive linkage of the points of discontinuous change. Compared to the Θ–DOF model the z–Θ–DOF model shows much lower amplitudes in Θ response. The region between the two points of discontinuous change is more expanded i.e. the spring–characteristic is more degressive than in the Θ–DOF model. A third difference between the two models is the local maximum of the Θ response at about $1/2\,\omega_{z,lin} = 1/2\sqrt{2k/m}$. This maximum is due to the coupling of Θ and z motion. Looking at the eigen frequency of the vertical motion it might be assumed that the z–motion is excited in a higher harmonic manner. For two given values of the forcing frequency fig. 14 shows the forced response for Θ and z. The one frequency was chosen to be $1/2\,\omega_{z,lin}$ the second to be $9\,1/s$ which is close to the right discontinuity of the z–Θ–DOF model. The time history results of the nonlinear model are compared to those of the linear one. For both forcing frequencies no vertical motion is excited for the linear model but for the nonlinear one. Whereas the left picture shows a pure second harmonic excitation the right picture includes further higher harmonics. Furthermore the nonlinear model shows a stationary shift Δz from the trimmed position $(F - mg)/(2k)$. Both phenomena can be explained by the perturbation method. Assume a nonlinear differential equation

$$\ddot{z} + \omega^2 z + \varepsilon z^2 = \hat{Q}\cos\Omega t. \tag{12}$$

The solution in z is in the form of a power series in ε. The coefficients of power of ε must balance and one obtains for the first two coefficients

$$\ddot{z}_0 + \omega^2 z_0 = \hat{Q}\cos\Omega t \tag{13}$$

$$\ddot{z}_1 + \omega^2 z_1 = -z_0. \tag{14}$$

The solution of equation 13 is

$$z_0 = \frac{\hat{Q}}{\omega^2 - \Omega^2}\cos\Omega t \tag{15}$$

and of equation 14

$$z_1 = -\frac{1}{2}\left[\frac{\hat{Q}}{\omega^2 - \Omega^2}\right]^2 \left[\frac{1}{\omega^2} + \frac{\cos 2\Omega t}{\omega^2 - 4\Omega^2}\right]. \tag{16}$$

The first term in 16 denotes a steady shift and the second term a second higher harmonic oscillation. For both simulation results it can be seen that z becomes negativ i.e. the body makes small jumps. The pitching motion at $\Omega = 1/2\,\omega_{z,lin}$ shows a harmonic oscillation but for $\Omega = 9\ 1/s$ further frequencies are involved. A FFT analysis has to show which ones are included. For both forcing frequencies the angle Θ of the nonlinear model shows a phase shift $\Delta\varphi$ to the linear model.

From that simple model some fundamental conclusions can be drawn which are listed below:

1) Θ–DOF model

- ω_Θ depends upon F/mg and $\hat{Q}$
- ω_Θ decreases smoothly with increasing F/mg
- the behavior of nonlinear system at low and high F/mg can be approximated by a linear system

$$F/mg \approx 0\%: \quad \omega_{0\Theta,nl} = a\sqrt{\frac{2k}{I_\Theta}} = \omega_{0\Theta,lin}$$

$$D_{\zeta,nl} = D_{\zeta,lin}$$

$$F/mg \approx 100\%: \quad \omega_{0\Theta,nl} = a\sqrt{\frac{k}{I_\Theta}} = \frac{\omega_{0\Theta,lin}}{\sqrt{2}}$$

$$D_{\zeta,nl} = \frac{D_{\zeta,lin}}{2}$$

- the behavior of the linear and nonlinear system is identical at low and high forcing frequencies

2) z–Θ–DOF model

- z– and Θ–DOF are coupled at medium forcing frequencies, z–DOF shows higher harmonic frequencies
- the response diagram shows extreme jump phenomena
- Θ–amplitude is lower than Θ–amplitude of the Θ–DOF model

4.2 Spatial model for transition considerations

After some insights into the behavior of nonlinear systems were given in the previous section the same description of the spring–damper–system used for the simplified model is applied to the spatial model of the helicopter. Parallel to that a linear landing gear modelling is used to show differences in the behavior of both modelling assumptions.

Following the conclusions drawn from the simplified model a reduction of body eigen frequencies due to the nonlinearity must be identifiable. Thus, several simulations with different rotor speeds were performed to investigate the dynamic behavior. An instability for the nonlinear model was detected at $\Omega = 87\%\,\Omega_{nom}$. The time history results are shown in fig. 15 where β and ζ are the blade flap and lead–lag angles in the rotating system. Thrust to weight ratio for this and the following calculations was set to $F/mg = 70\%$. An initial disturbance was applied to the pitch angle and was chosen to be $\Theta = 0.95°$. The linear model behaves stable but due to the low lead–lag damping the oscillation for the linear model vanishes slowly. In opposite to that the oscillation for the nonlinear model increases dramatically. The oscillation looks irregularly and shows an explosive character. The behavior of the system depends strongly upon the initial conditions. Applying the same initial disturbance to the roll angle it does not lead to an instability. The same can be seen reducing the initial value for the pitch angle. Increasing the initial pitch angle that leads to a rapid destabilization of the system within 30 rotor revolutions or even faster, depending upon the initial disturbance. For linear self–excited systems it is known that already infinitesimal disturbances lead to an oncomming instability. Nonlinear systems behave differently depending upon the nonlinear quality. A certain amount of initial disturbance is necessary to destabilize the system. For low disturbances linear and nonlinear models behave similarly. This can be explained as follows: Due to $F/mg < 100\%$ the trimmed solution for $z > 0$. All four spring–damper–systems are compressed. To relax and lift the both front spring–damper–systems a pitch angle Θ is needed which can be computed from the trimmed z attitude divided by the spring–damper–offset from the c.g. For lower pitch angles both front spring–damper–systems are still compressed. Thus, the nonlinear system shows a linear behavior.

From fig. 4 it is known that the linear model shows an instability at $\Omega = 91\%\,\Omega_{nom}$. The time history is plotted in fig. 16. This time the linear model shows the predicted instability whereas the nonlinear does not. But still the instability of the linear system does not show an explosive character. From the ground resonance test results shown in [7] ground resonance is known to be a strong instability for articulated rotor helicopters. In this study the lead–lag angle needs 50 rotor revolutions (about 8 seconds) till its amplitude increases to 2°. Opposite to the linear model the nonlinear shows no instability for these operating conditions. After a transient oscillation the motions show an almost constant vibrational amplitude. The reason for that is a persistent change of linear and nonlinear characteristics. If the model shows linear characteristics the chosen rotor speed will lead to an oncomming instability. The vibrational amplitudes increase until a nonlinear behavior occurs. Due to the nonlinearities the eigen frequencies shift, the oscillation is no longer self–excited, the amplitudes drop and the process starts at the beginning. From this it becomes clear that this is not a stable but a highly sensitive process. A slight increase of the initial disturbance leads again to a dramatic instability.

Finally it has to be tested whether the optimized controllers are sufficient to suppress an oncomming instability or not. On behalf of the two studied rotor speeds fig. 17 shows the closed loop simulation results at $\Omega = 91\%\,\Omega_{nom}$. The controller chosen for this simulation was C2 from fig. 10. Although optimized for a thrust to weight ratio of 50% the controller is successful in stabilizing the linear model. The results are as good as those of ref. [8]. Looking at the control activity this controller is even better, since the control amplitude does not reach 1° whereas it is about 2° in ref. [8]. Applying the same controller to the nonlinear model this leads to a considerable instability within 28 rotor revolutions although the open loop system showed a neutral behavior. This is due to the high feedback gains and the high moment capacity of the hingeless rotor. Because of the initial pitch disturbance (pitch up) the controller generates a restoring rotor moment. The fuselage pitches down but shoots over and the rear spring–damper–systems lose ground contact. Since the controller has been designed for a linear system all four spring–damper–systems are expected to generate restoring moments. Since only the front springs generate these restoring moments this results in a further over–shoot of fuselage over its neutral position. After the pitch down motion has been stopped the same happens during pitching up. Due to the control inputs the flapping motion is excited considerably and due to flapping and

the fuselage motion lead–lag as well. To test the influence of thrust to weight ratio on the closed loop system stability F/mg was varied systematically. All other values were kept constant. It was found out that the controller C2 could stabilize the nonlinear model at both investigated rotor speeds $\Omega = 87\%\,\Omega_{nom}$ and $91\%\,\Omega_{nom}$ up to $F/mg = 68\%$. Now instability occured for the linear model within the whole range of F/mg at the critical rotorspeed $\Omega = 91\%\,\Omega_{nom}$. From this it becomes evident that active control is possible even if the described nonlinearities are included in the modelling assumptions. Since the lead–lag motion grows rapidly the feedback gains of the cyclic lead–lag angles were reduced by 1/4 and of the lead–lag velocities by 1/10. Roll rate gain was reduced by 1/3. All phase angles were kept at their optimized values. Finally fig. 18 shows the closed loop time history for both investigated models with the modified controller at $\Omega = 91\%\,\Omega_{nom}$. Similar results were obtained at $\Omega = 87\%\,\Omega_{nom}$ using the same controller. Due to the reduction of feedback gains the model with the linear landing gear shows a less stable but still sufficient behavior compared to fig. 17 and the model with the nonlinear landing gear is stabilized this time.

5 Outlook and Conclusion

The intent of the presented investigation was to demonstrate the possibilities of active control to suppress ground resonance and to provide an insight into the behavior of nonlinear systems. Modelling of nonlinearities is important to describe the helicopter during transition from ground to air. The nonlinearities being modelled in this study dealt with nonlinear spring–damper–characteristics of the landing gear. The characteristics were formulated analytically. With this a simple way was found out to specify the possibility of losing ground contact and to include the nonlinear landing gear description as well as the linear one in the same numerical integration routine. The helicopter model with the linear landing gear description was linearized and transformed into state space representation.

Taking the linearized model as a basis an eigen value computation was performed variing the rotor speed from 0 to $140\%\,\Omega_{nom}$. Since a low lead–lag damping constant was chosen two instabilities occured. The one at $91\%\,\Omega_{nom}$ due to a coupling between ζ_{reg} and x/Θ mode the other at $112\%\,\Omega_{nom}$ due to a coupling between ζ_{reg} and y/Φ mode. Even a third instability occured which was not further considered for this study. It turned out that the same model was free from air resonance.

Different controllers were optimized using a SAS structure. Single variable feedback was not sufficient in stabilizing ground resonance. As demonstrated with a root locus plot ζ_{prog} became unstable with increasing feedback gain. Very promising results were obtained using multi–variable feedback of the cyclic lead–lag, roll and pitch states. Two controllers were designed at the two critical rotor speeds and provided sufficient stability margins to the system. None of these controllers could achieve stability throughout the considered rotor speed range. Thus, additional feedback of longitudinal and lateral translational velocity was included to the controller design. With this stability for all rotor speeds was obtained. Applying the optimized controllers to the helicopter in hover this led to a dramatic destabilization because of the high feedback gains. Important aspects and questions for further research of active control of ground and air resonance are:

- To keep the complexity of the active device low it has to be investigated which states are at least necessary for stabilizing ground and air resonance. This is especially valid for the rotor states.
- Is it possible to design a controller for ground resonance without scheduling the feedback gains and phases with rotor speed and thrust to weight ratio (collective pitch)?
- Is the designed controller robust enough to handle all possible operating conditions (weight, offset of c.g. from rotor axis etc.)?
- To avoid adverse effects of the ground and air resonance devices on handling qualities and on classical stability filtering of feedback signals has to be investigated in more detail.
- How can the transition from ground to air be handled since the helicopter needs a very short time to become airborne and since nonlinear behavior may occur during transition?

Regarding this it becomes obvious that further systematic studies have to be carried out in order to explore the full potential of active control of aeromechanical instabilities and to investigate the impact of nonlinearities on the dynamic behavior of the helicopter.

Picking up the last aspect the second part of this paper dealt with the differences between a linear and nonlinear modelling approach. First, a simple plane model was considered to gain physical insight into the

system. Secondly, the spatial model was investigated. Simulation results were used to show differences in behavior. The behavior of the linear and nonlinear model depended upon the operating conditions (rotor speed and thrust to weight ratio). In addition to that the behavior of the nonlinear model depended upon the initial disturbance whereas the behavior of the linaer model does not. Due to the degressive character of the formulated nonlinearity an instability arose at $\Omega = 87\%\,\Omega_{nom}$. The instability at $\Omega = 91\%\,\Omega_{nom}$ predicted with the linearized model seemed to vanish but a higher initial disturbance led again to an instability. The nonlinear model may regarded to be unstable within a broad range of rotor speed whereas the linear model is unstable within a "small" band arround the critical rotor speed.

Applying a previous optimized controller to the helicopter with the linear landing gear showed sufficient stability and low control activities. Opposite to that the helicopter with the nonlinear landing gear became dramatically unstable but stability could be achieved for both linear and nonlinear model by reducing several feedback gains. This may be a hint that filtering is possible to stabilize the helicopter during transition but further effort has to be made to investigate the behavior of nonlinar systems.

6 References

[1] J. Ewald. *Untersuchung zur aeromechanischen Stabilität des Hubschraubers.* ZLR–Forschungsbericht 91–05, Zentrum f"ur Luft– und Raumfahrttechnik der Technischen Universität Braunschweig, Braunschweig, 1991.

[2] W. Johnson. Influence of unsteady aerodynamics on hingeless rotor ground resonance. *Journal of Aircraft*, 19(8):668 – 673, 1982.

[3] H.C. Curtiss Jr. Stability and control modelling. *Vertica*, 12(4):381 – 394, 1988.

[4] D.W. Jordan, P. Smith. *Nonlinear Ordinary Differential Equations.* Oxford University Press, 1977.

[5] F.K. Straub, W. Warmbrodt. The use of active controls to augment rotor/fuselage stability. *Journal of the American Helicopter Society*, 30(3):13 – 22, July 1985.

[6] G. Reichert, H. Huber. Influence of elastic coupling effects on the handling qualities of a hingeless rotor helicopter. *AGARD CP – 121*, pages 8.1 – 8.15, February 1973.

[7] G. Reichert, J. Ewald. Helicopter ground and air resonance dynamics. *Fourteenth European Rotorcraft Forum*, Milano, Italy, pages 43.1 – 43.12, September 20 – 23 1988.

[8] G. Reichert, U. Arnold. Active control of helicopter ground and air resonance. *Sixteenth European Rotorcraft Forum*, Glasgow, Scotland, pages III.6.2.1 – III.6.2.14, September 18 – 20 1990.

[9] M.D. Takahashi, P.P Friedmann. Design of a simple active controller to suppress helicopter air resonance. *44th Annual Forum of the American Helicopter Society*, pages 305 – 315, June 1988.

[10] M.D. Takahashi, P.P Friedmann. A model for active control of helicopter air resonance in hover and forward flight. *Fourteenth European Rotorcraft Forum*, Milano, Italy, pages 57.1 – 57.23, September 20 – 23 1988.

[11] M.I. Young, D.J. Bailey. Stability and control of hingeless rotor helicopter ground resonance. *Journal of Aircraft*, 11(6):333 – 339, June 1974.

[12] M.I. Young, D.J. Bailey, M.S. Hirschbein. Open and closed loop stability of hingeless rotor helicopter air and ground resonance. *AHS/NASA–Ames Specialists' Meeting on Rotorcraft Dynamics*, February 13 – 15 1974.

[13] R.E. Donham, S.V. Cardinale, I.B. Sachs. Ground and air resonance characteristics of a soft in–plane rigid–rotor system. *Journal of the American Helicopter Society*, 14(4):33 – 41, October 1969.

[14] W.S.Levine, M. Athenas. The determination of the optimal constant output feedback gains for linear multivariable systems. *IEEE Transactions on Automatic Control*, 15(1):44 – 48, February 1970.

[15] R.A. Ormiston. Rotor–fuselage dynamics of helicopter air and ground resonance. *Journal of the American Helicopter Society*, 36(2):3 – 20, April 1991.

[16] F.K. Straub. Optimal control of helicopter aeromechanical stability. *Eleventh European Rotorcraft Forum*, London, England, pages 77.1 – 77.16, September 10-13 1985.

[17] M. E. Wasikowski. *Optimal Output Vector Feedback, Theory Manual.* Georgia Tech Research Institute, Georgia USA, 1992.

Controller	$\dot{\zeta}_C$	$\dot{\zeta}_S$	ζ_C	ζ_S	u_{kS}	v_{kS}	p_S	q_S	Φ	Θ
C1	0.07 s	0.08 s	0.25	1.30	0.07 s/m	0.08 s/m	0.25 s	0.33 s	3.60	1.10
	221°	250°	102°	180°	167°	178°	141°	20°	105°	341°
C2	0.05 s	0.11 s	1.08	1.72	–	–	0.04 s	0.09 s	1.44	0.81
	230°	261°	42°	225°	–	–	199°	59°	123°	339°
C3	0.08 s	0.08 s	1.77	1.54	–	–	0.07 s	0.03 s	2.47	0.22
	194°	244°	107°	130°	–	–	199°	59°	59°	55°

Table 2: Optimized Feedback Gains and Phases

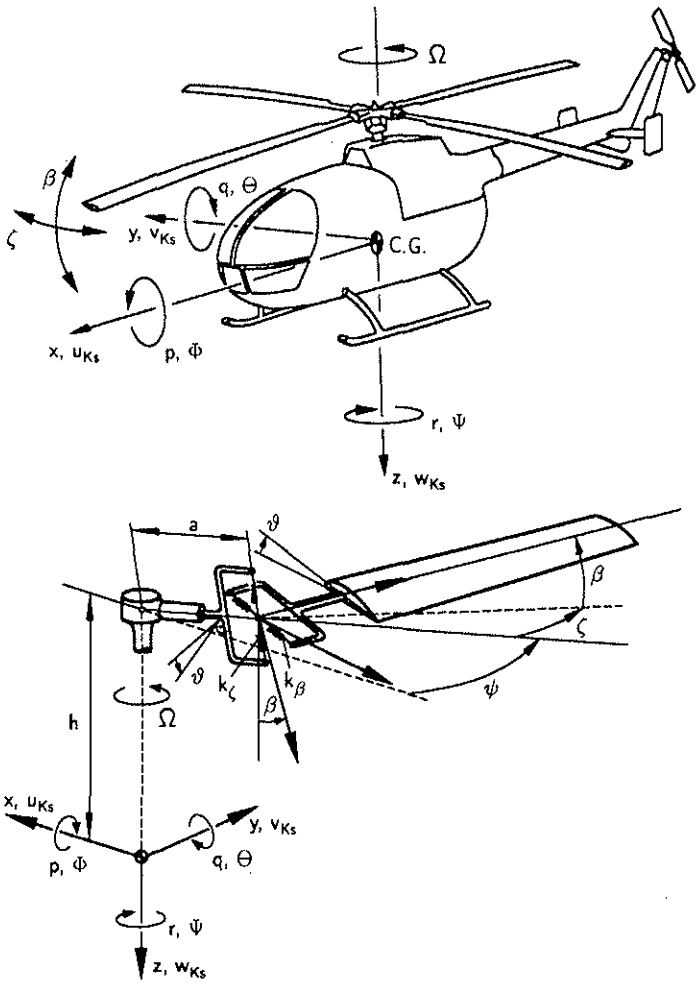

Figure 1: Mathematical Helicopter Model

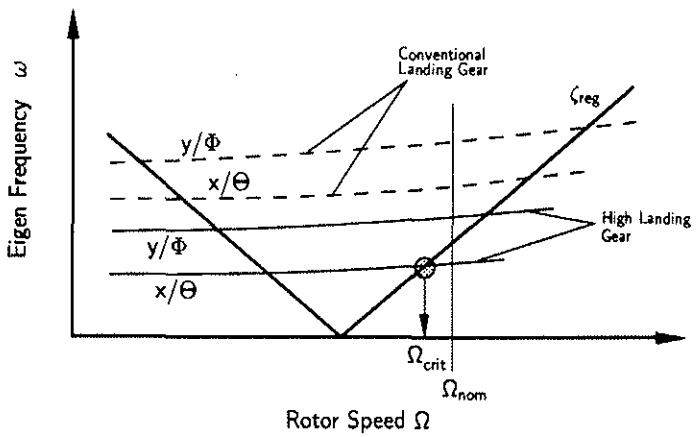

Figure 2: Principle Eigen Frequencies of Different Landing Gear Types

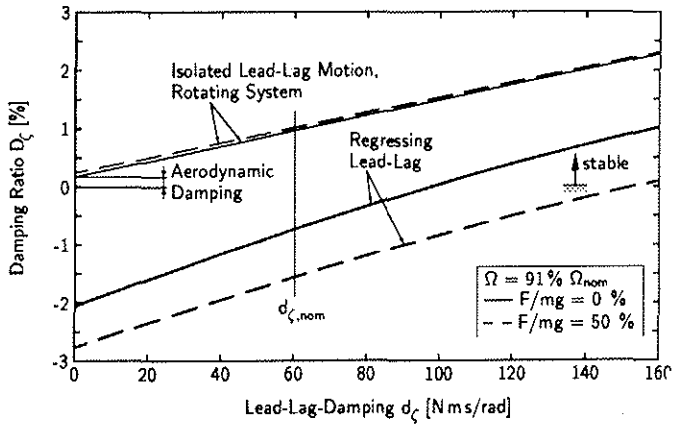

Figure 3: Damping Ratio D_ζ vs. Lead–Lag Damping d_ζ for the Isolated Lead-Lag Motion and Regressing Lead-Lag of the Coupled Rotor-Body System

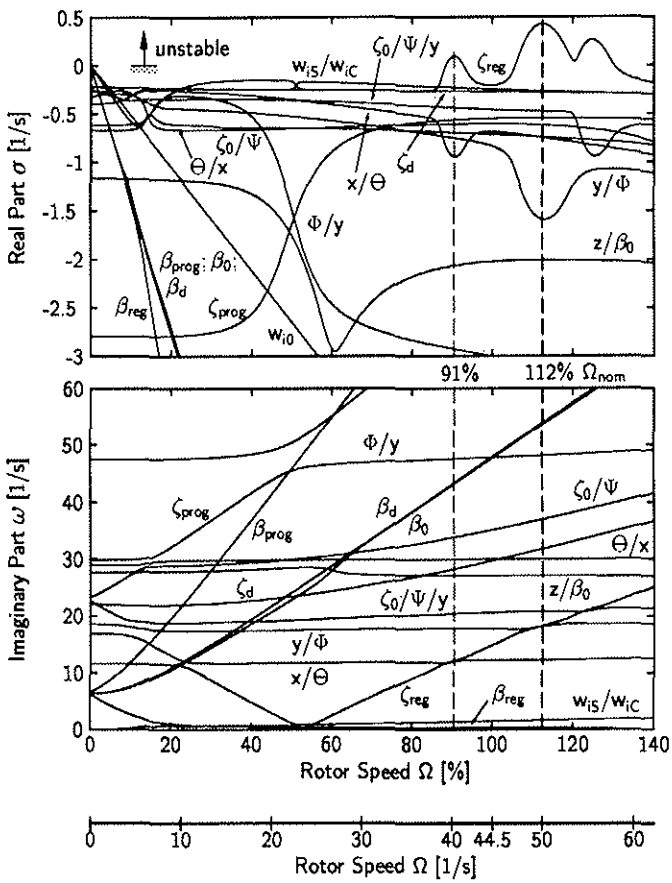

Figure 4: Eigen Values of the Coupled Rotor-Body-System on Ground, High Landing Gear, F/mg = 0%

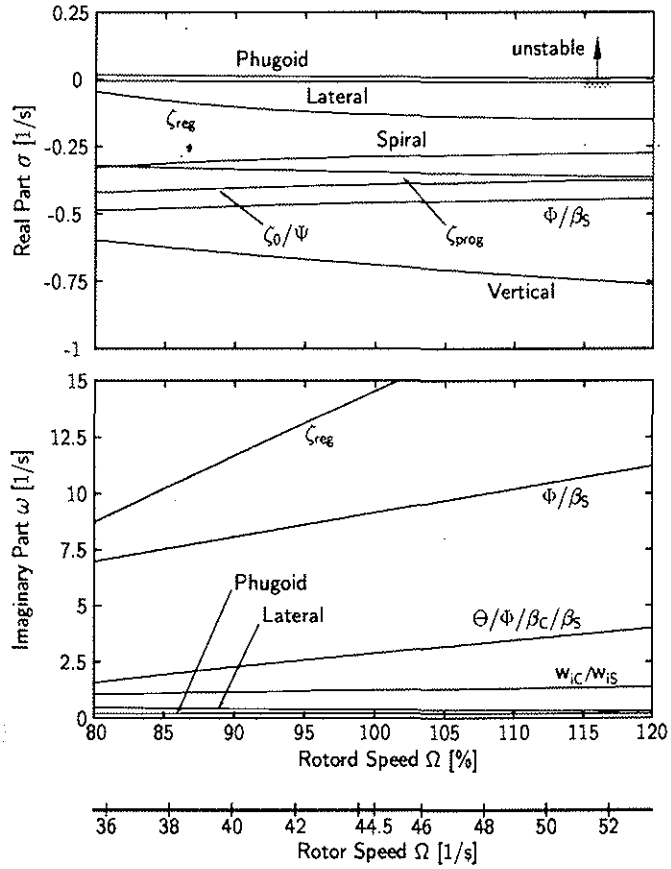

Figure 5: Eigen Values of the Coupled Rotor-Body-System in Hover, F/mg = 100%

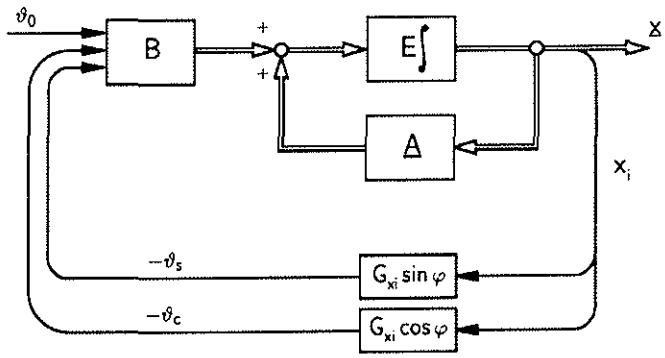

Figure 7: SAS-Principle

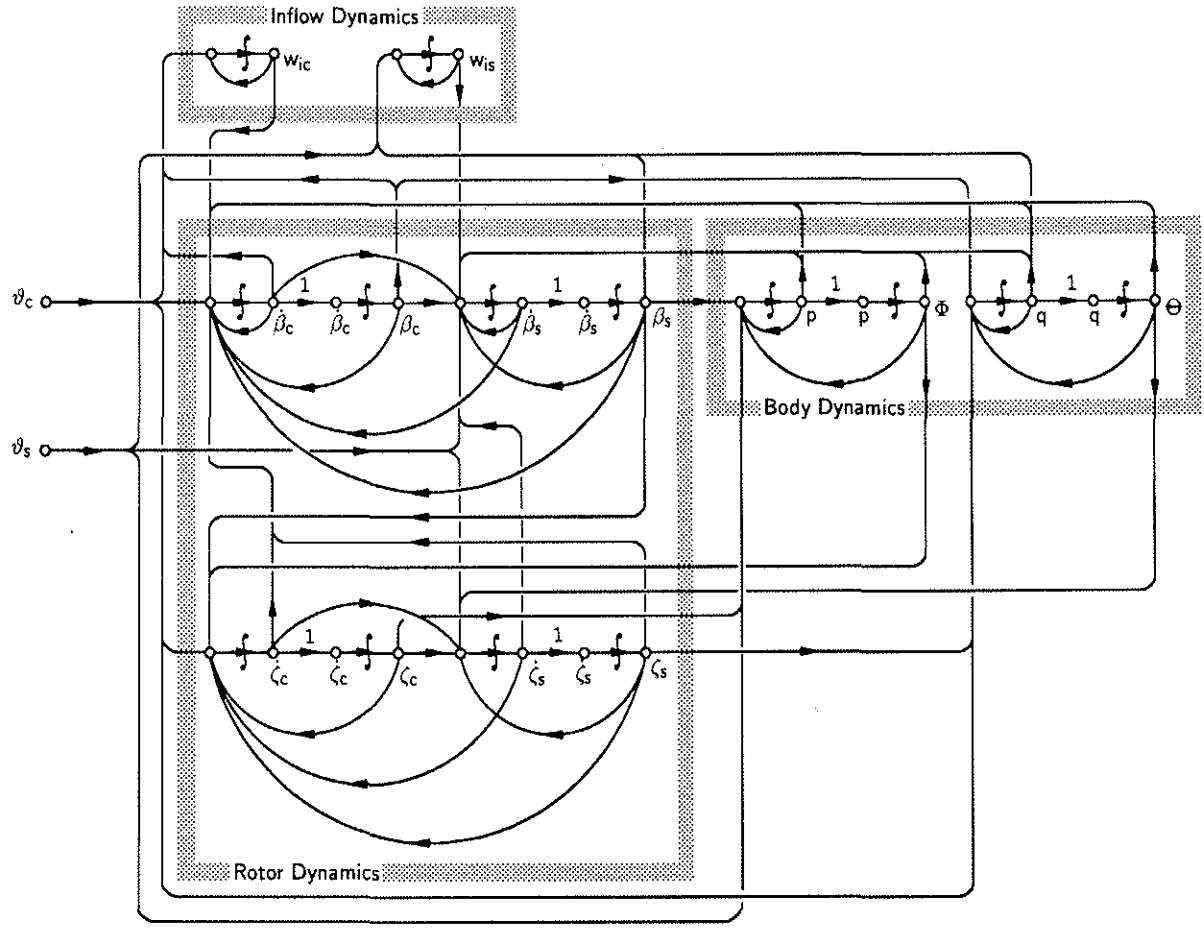

Figure 6: Signal Flow Diagram for Simplified Ground Resonance Considerations

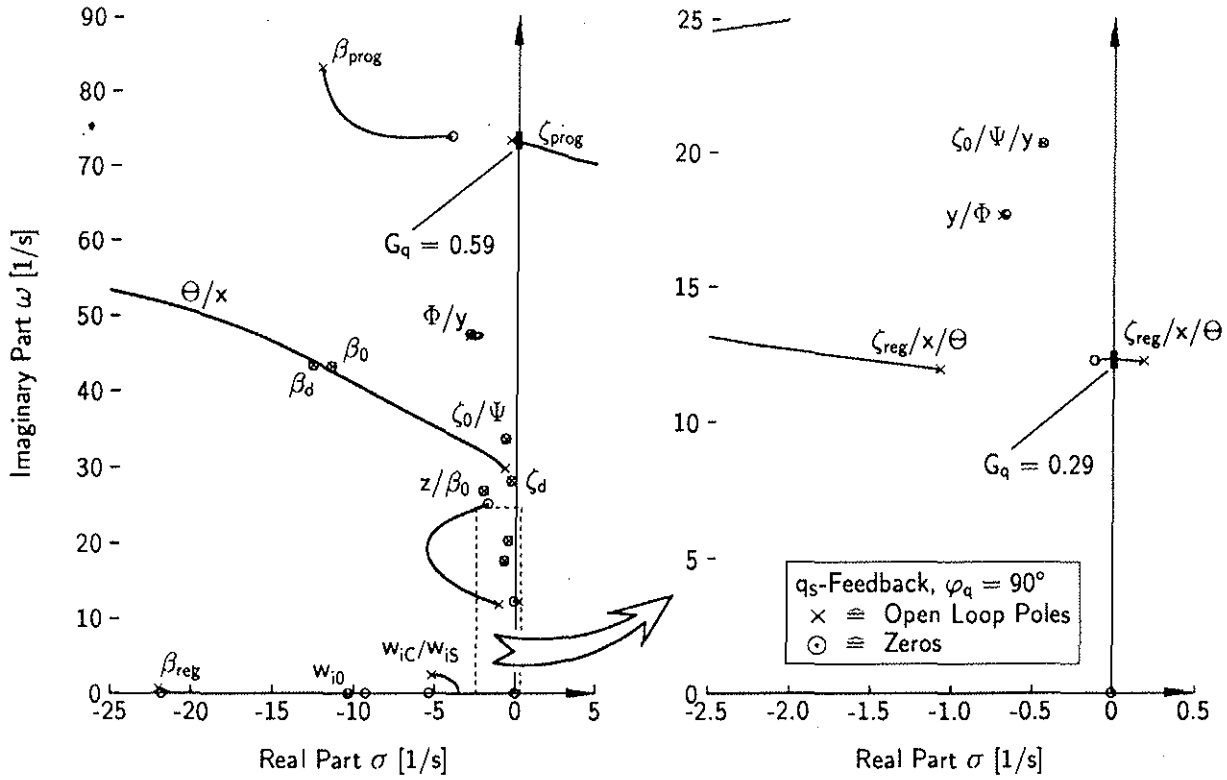

Figure 8: Root Locus for Pitch Rate Feedback, $\Omega = 91\%\,\Omega_{nom}, F/mg = 50\%$

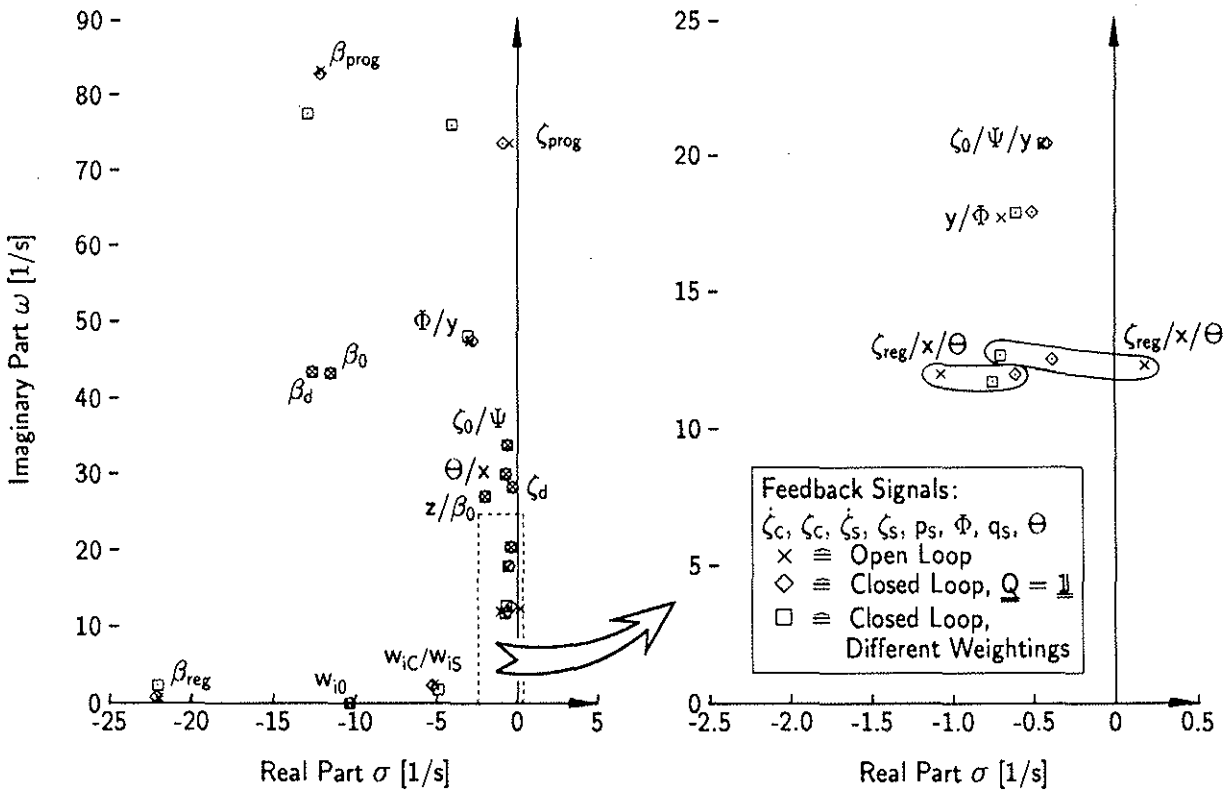

Figure 9: Eigen Values for Mult-Variable Feedback, $\Omega = 91\%\,\Omega_{nom}, F/mg = 50\%$

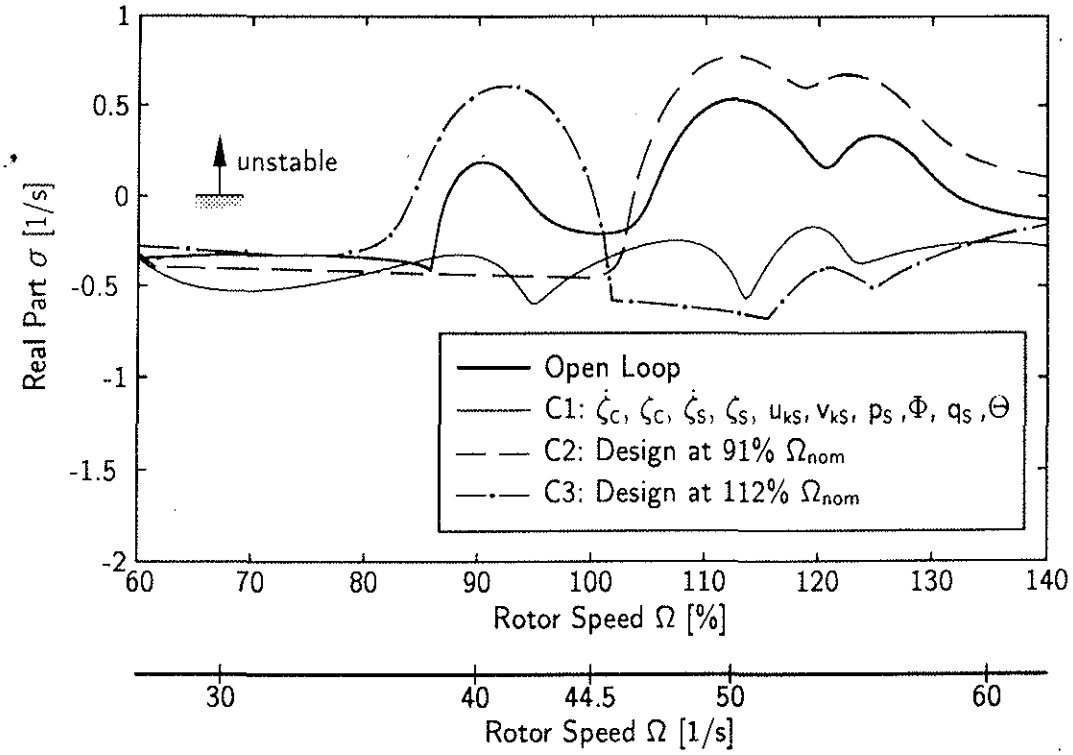

Figure 10: Aeromechanical Stability of Least Stable Mode vs. Rotor Speed, $F/mg = 50\%$

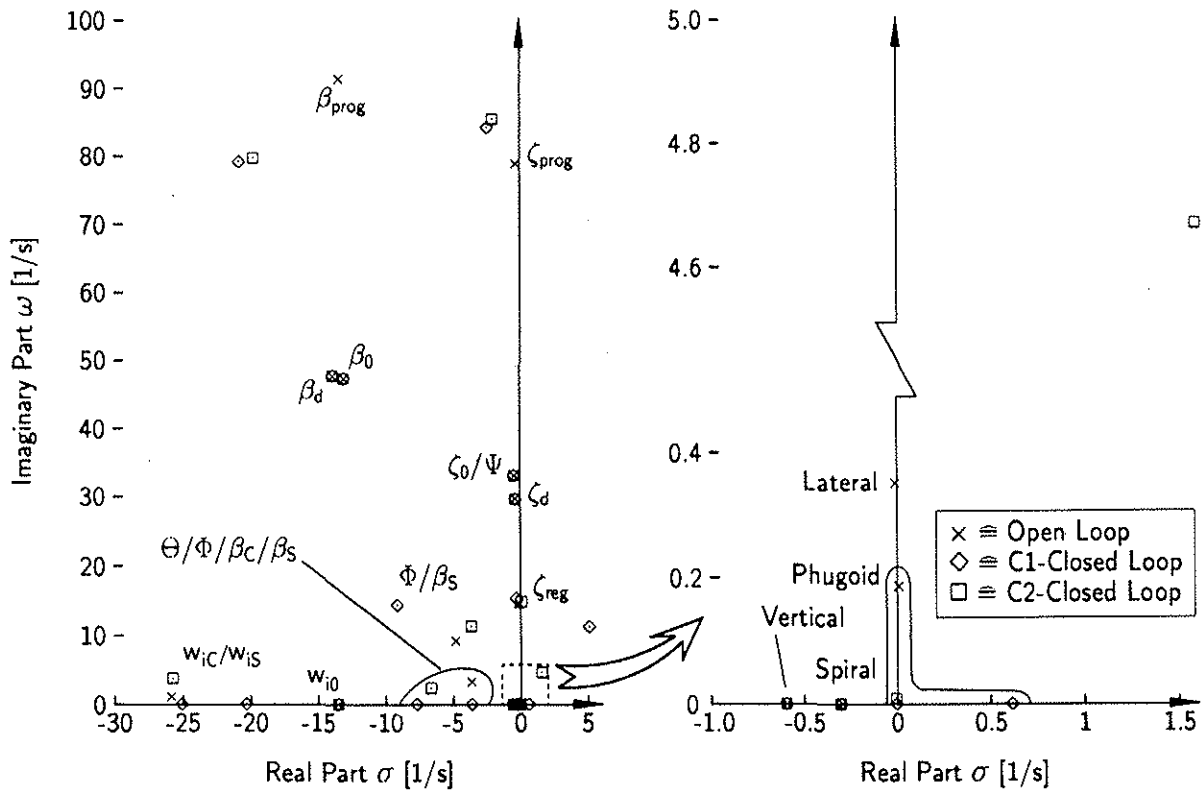

Figure 11: Open and Closed Loop Root Placement for Helicopter in Hover

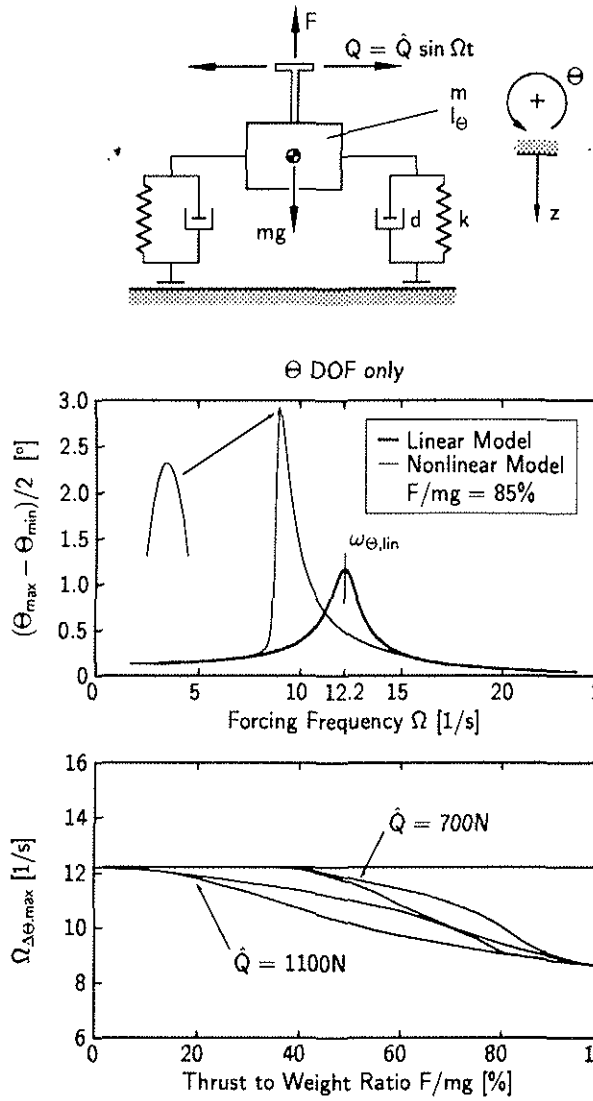

Figure 12: Simplified Model for Transition from Ground to Air

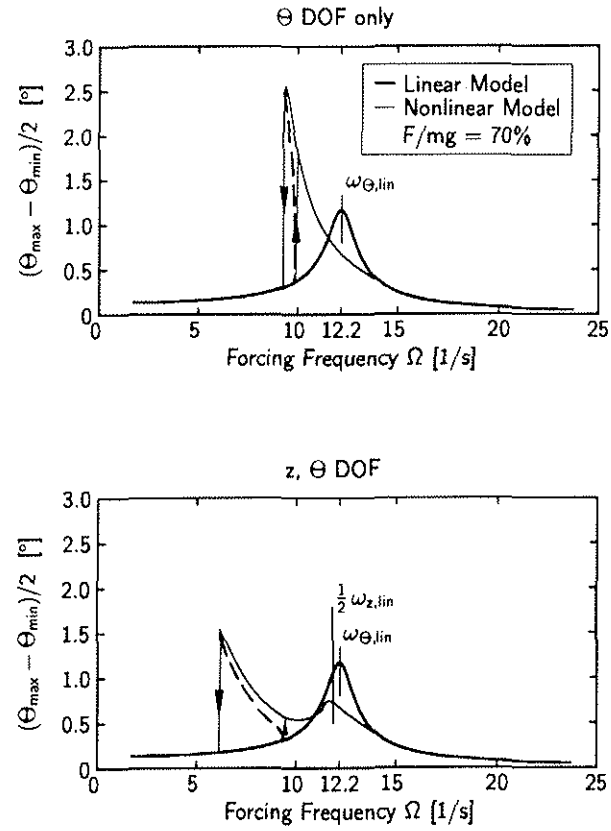

Figure 13: Response Diagram for Θ and z, Θ DOF-Model, $\hat{Q} = 1100\ N$

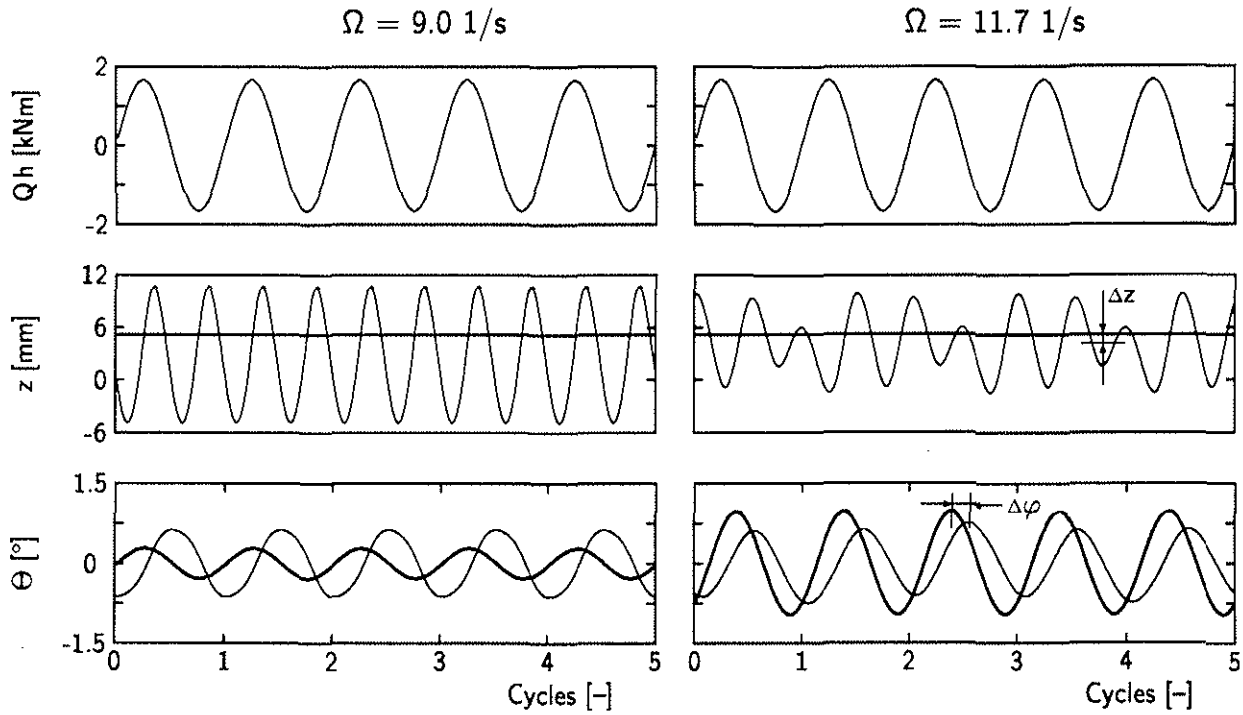

Figure 14: Forced Response of Linear and Nonlinear Model, $F/mg = 70\%$, $\hat{Q} = 1100\,N$, — Linear Model, — Nonlinear Model

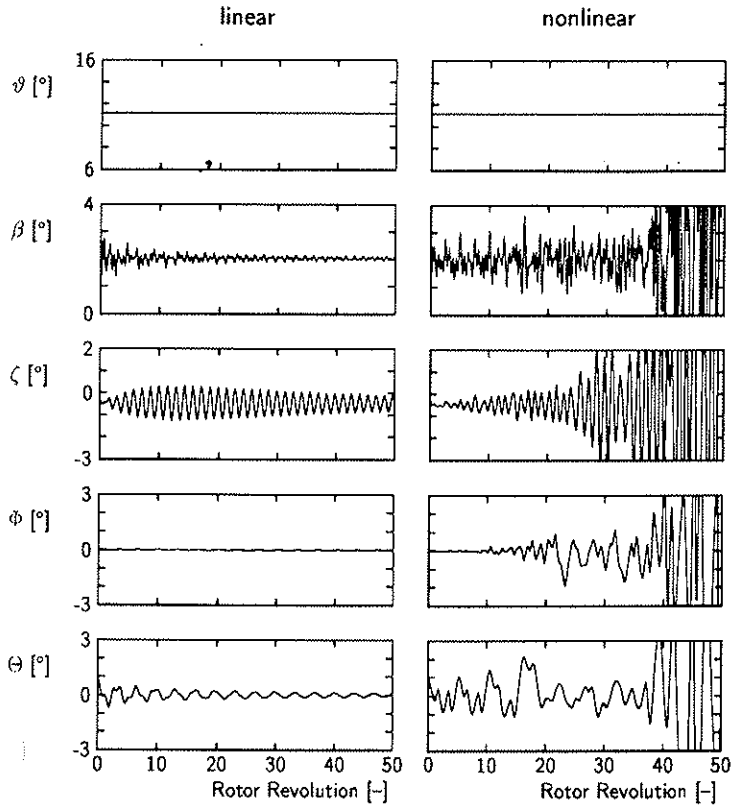

Figure 15: Transient Response with Linear and Nonlinear Landing Gear Model, $\Omega = 87\,\%\,\Omega_{nom}$, $F/mg = 70\,\%$

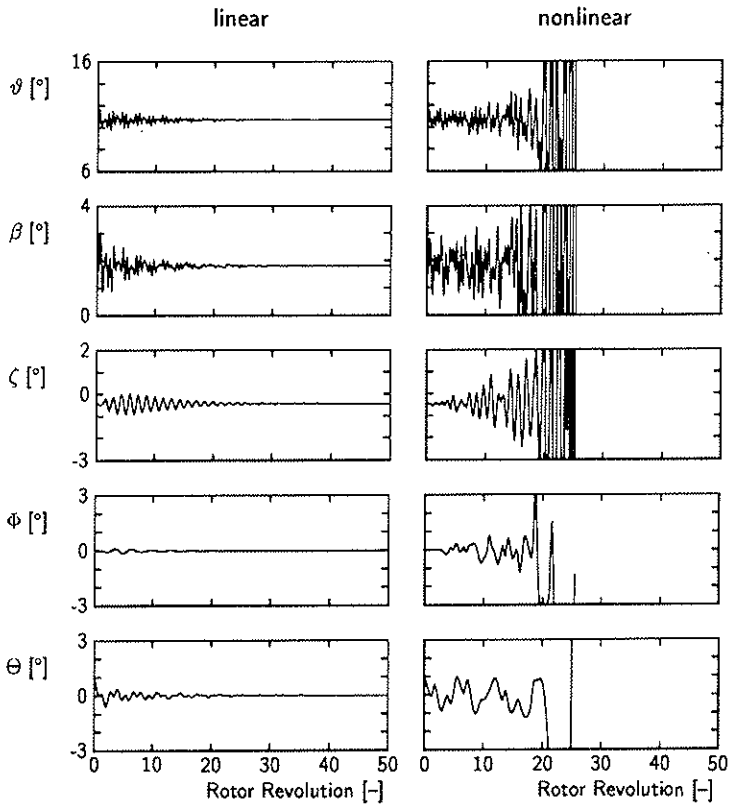

Figure 17: Closed Loop Transient Response with Linear and Nonlinear Landing Gear Model, $\Omega = 91\,\%\,\Omega_{nom}$, $F/mg = 70\,\%$, Controller C2

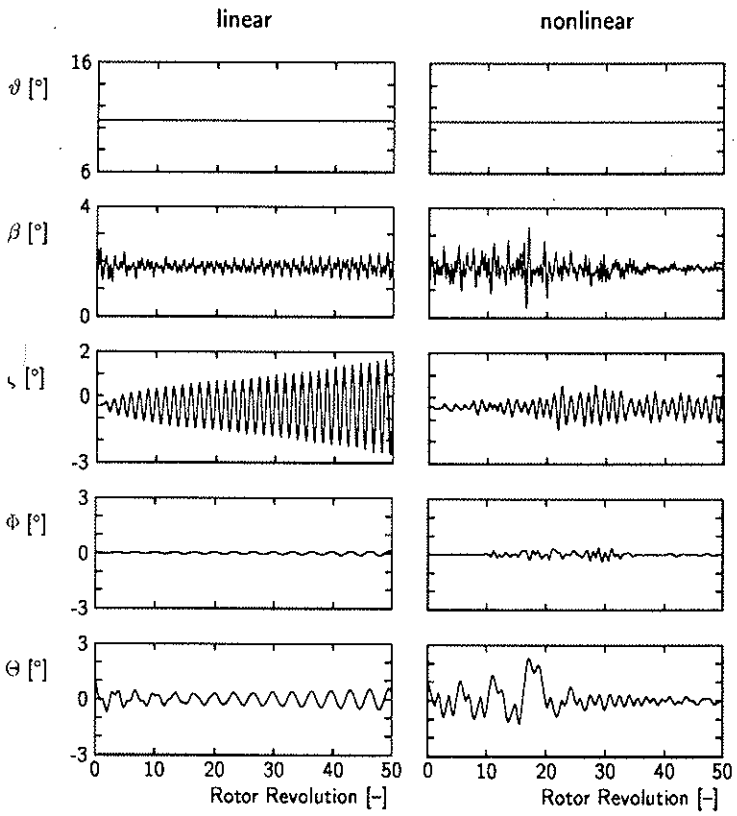

Figure 16: Transient Response with Linear and Nonlinear Landing Gear Model, $\Omega = 91\,\%\,\Omega_{nom}$, $F/mg = 70\,\%$

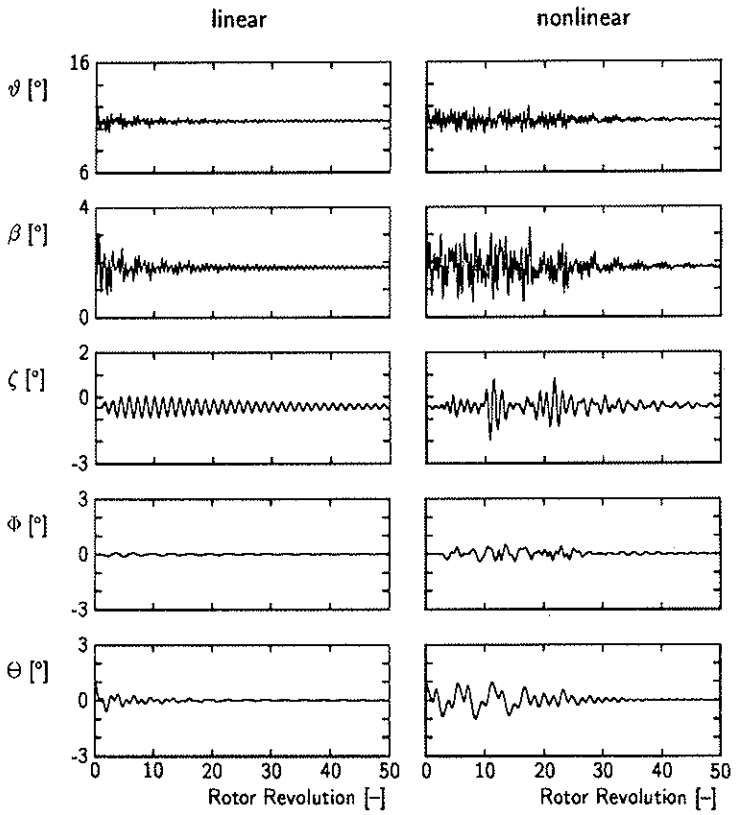

Figure 18: Closed Loop Transient Response with Linear and Nonlinear Landing Gear Model, $\Omega = 91\,\%\,\Omega_{nom}$, $F/mg = 70\,\%$, Modified Controller C2